Effects of three-dimensional atomic forces in topographical imaging of atoms with an atom force microscope

Wei Li Wang, S. Jack Hu, and Roy Clarke
The University of Michigan, Ann Arbor, Michigan 48105, USA
(Received 12 May 2003; published 2 December 2003)

A scanning tip on a surface is subject to the normal load and the scan direction friction force. This macroscopic model, however, breaks down for atomic-resolution imaging in an atom force microscope (AFM) where the friction was found to be two dimensional. In this paper, a simple model is introduced to describe how these three-dimensional atomic forces and the induced deflections are coupled through tip-cantilever force sensors. In particular, we discuss a mechanism leading to an unexpected residual linear deflection due to the two-dimensional lateral forces, which could be the main cause preventing optical-beam-deflection AFM's from obtaining true images of atoms in the contact mode. With this mechanism, some ''topography'' images of surface atomic structure previously observed can be interpreted as maps of the lateral force in the longitudinal direction. Some puzzling features such as the well-known ''resolution of every other atom'' of graphite topographical images can be readily explained.

DOI: 10.1103/PhysRevB.68.245401 PACS number(s): 68.37.Ps, 68.35.Bs, 68.35.Af

I. INTRODUCTION

Ever since the invention of the atom force microscope[1] (AFM), numerous attempts have been made to demonstrate its capability in imaging atoms. Binnig *et al.*[2] successfully obtained the lattice image of a graphite surface with a corner of the cantilever, i.e., without a sharp tip. In the same year, Marti *et al.*[3] also observed the hexagonal structure on a highly oriented pyrolytic graphite (HOPG) surface using a uniquely designed AFM with the sample covered by paraffin oil. Meyer and Amer[4,5] imaged the fcc structure of a NaCl (001) surface in an ultrahigh vacuum (UHV) with an optical-beam-deflection AFM, the type of design that subsequently became commercially available and hence the most widely used. AFM was believed to be capable of resolving surface structures of both conductors and insulators on the atomic scale in ambient atmosphere, UHV, and aqueous environments. However, just as there were many successes, there are many questions left with no definite answer. One of them is that many topographical images of the graphite surface show only three peaks per hexagonal ring, which has been interpreted as the ''atomic resolution of every other atom.'' [6] There are several possible explanations—however, with little convincing supporting evidence.

Basically, an AFM detects atoms by means of atom forces. It is understandable that the AFM also became an extremely useful tool in surface tribological studies.[7] One year after the invention of the AFM, Mate *et al.*[8] first studied atomic-scale friction and found that the frictional force images exhibited the periodicity of the unit cell of the surface and attributed this observation to the ''stick-slip'' phenomenon. Fujisawa *et al.*[9–11] pointed out that the atomic stick-slip motion is not one dimensional but two dimensional, referring to the corresponding lateral forces as ''two-dimensional'' friction forces in contrast to the traditional one-dimensional macroscopic friction. Ruan and Buhshan[6] argued that the two-dimensional lateral forces are intrinsic, not necessarily dependent on the stick-slip motion. They also compared the simultaneously obtained ''topography'' and friction force maps of the graphite surface and analyzed the shift between the peaks of the ''topography'' and the friction in the scan direction. Besides the ''resolution of every other atom,'' their measurement showed an anomalously large corrugation amplitude which was not clarified. Hölscher *et al.*[12] studied the movement of a tip on a graphite surface by measuring and simulating lateral force maps. It was identified that the force maps represent a ''hollow-site resolution'' instead of the ''resolution of every other atom'' because the tip can only profile the hollow sites due to the stick-slip movement.

In this paper, we attempt to link the topographical AFM images of atoms with the three-dimensional atom forces using a simple model. In Sec. II, we start with an illustration of the three-dimensional nature of the atom forces on a surface, and then in Sec. III, we describe how these forces and the induced deflections are coupled during atomic-scale topographical imaging, analyzing them using a simple cantilever model. In Sec. IV, the simulation and experiment results are discussed, followed by conclusions in Sec. V.

II. THREE-DIMENSIONAL ATOM FORCES AND TIP DEFLECTION ON A SURFACE

The interaction forces between a scanning tip and a substrate in contact are rather complicated. However, in practice, because the scan speed is much slower than the vibrational speed of atoms and the tip dynamics, we choose to treat the system as if it is in equilibrium at all times and ignore the nonconservative frictional forces due to phonon propagation, etc. Also neglected are the atomic dynamics and surface deformation. Regardless of their simplicity, such conditions have been assumed in previous studies and many experimental results were successfully reproduced.[13] Even with such simplifications, the interaction could still be complicated by the coexistence of several types of long-range macroscopic forces and short-range repulsive forces—namely, electrostatic, magnetic, van der Waals, and chemical interactions.

However, for contact-mode imaging, the tip is often placed in the short-range repulsive-force-dominant regime, and in this case, one can neglect the long-range forces and assume only the two layers of atoms at the contact surface play an important role. Therefore, in the following calculation, we consider a layer of substrate atoms in contact with a layer of tip atoms scanned at a constant height.

In the interaction potential field of the substrate, the periodic potential of a tip primitive lattice cell at position $\vec{r}$ can be written as the summation of its Fourier components:

$$V(\vec{r}) = \sum_G V_G \exp(i\vec{G}\cdot\vec{r}). \tag{1}$$

The two-dimensional reciprocal lattice vectors $\vec{G} = v_1\vec{b}_1 + v_2\vec{b}_2$ (v_1 and v_2 are integers) satisfy $\vec{b}_i\cdot\vec{a}_i = 2\pi\delta_{ij}$, where $\vec{a}_j$ is the jth primitive lattice vector of the substrate crystal. A contact layer with m lattice cells has a total potential of

$$V_t = \sum_m \sum_G V_G \exp(i\vec{G}\cdot\vec{r}_m), \tag{2}$$

where the position of each individual cell, $\vec{r}_m = \vec{r}_0 + \vec{T}$, is the summation of the nominal tip position $\vec{r}_0$ and a crystal translation vector of the tip lattice $\vec{T}$. A special case is that $\vec{T} = u_1\vec{a}_1 + u_2\vec{a}_2$ (u_1 and u_2 are integers), and Eq. (2) becomes

$$V_t = \sum_m \sum_G V_G \exp(i\vec{G}\cdot\vec{r}_0)\cdot\exp(i\vec{G}\cdot\vec{T}). \tag{3}$$

But $\exp(i\vec{G}\cdot\vec{T}) = 1$ because $\vec{G}\cdot\vec{T} = 2\pi(v_1u_1 + v_2u_2)$; the total potential is thus given by

$$V_t = m\sum_G V_G \exp(i\vec{G}\cdot\vec{r}_0). \tag{4}$$

This is the case when the most significant interaction occurs. The coherent interaction results in large corrugations of the total potential which increase linearly with the number of the tip atoms. However, a more general case is $\vec{T} \neq u_1\vec{a}_1 + u_2\vec{a}_2$ and each term $\exp(i\vec{G}\cdot\vec{T})$ in Eq. (3) contributes a phase error to the sum so that the total potential is flattened. As an example, Fig. 1 illustrates the calculated interaction potential map of a 28-graphite-atom single layer scanning over a substrate layer of the same kind with 984 carbon atoms. For case (a), the tip and the substrate are commensurate as described by Eq. (4) while in (b) the tip is rotated by 30° and shows a flattening effect by an order of magnitude.

Meanwhile, if the tip is attached to springs which are flexible in both x and y directions, the potential of the springs under elastic deformation and the potential of the tip-substrate interaction can be superimposed and plotted versus the x, y direction deflections as shown in Fig. 2(c). Clearly, the tip in the equilibrium state could stick at one of the local minima around the equilibrium position of the tip and result in two-dimensional deflections and induced forces. In practice, due to the strong spring stiffness, limited vertical load, and flattening effect mentioned above, the tip sticks usually no more than several lattice constants away from the equilibrium position. Such a phenomenon was observed previously in lateral force microscope (LFM) friction studies, and double (lattice constant) stick-slip has been reported.[9] For a tip with large enough stiffness and/or small enough load, the number of minima reduces to one which is within a sublattice distance from the tip equilibrium position, and then stick-slip does not occur.

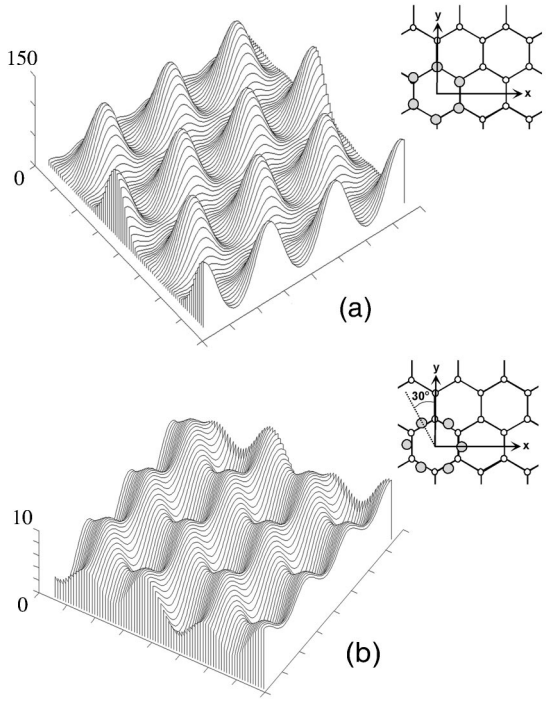

FIG. 1. The potential map (in arbitrary units) of a single-layered graphite tip (large circles) scanning over a graphite substrate layer (small circles) with a scan size of 7.4 Å by 7.4 Å. In (a), the tip and the substrate are commensurate while in (b) the tip is rotated by 30° before scanning. A pairwise Lennard-Jones potential is used for the calculation.

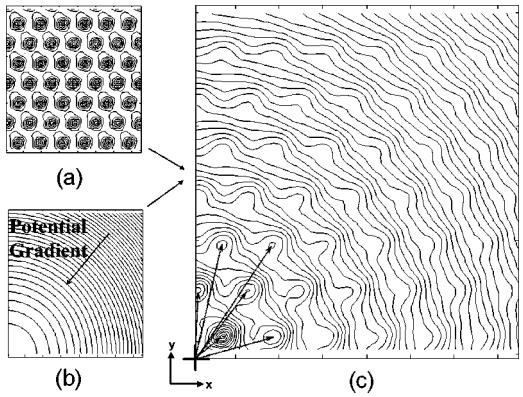

FIG. 2. (a) Calculated corrugations of the tip substrate interaction potential, which is equivalent to that of Fig. 1(b). (b) Potential contour lines of a tip that can elastically deflect in both x and y directions. (c) The superposition of (a) and (b) indicates the local minima where the tip could stick. Left lower corner is the tip equilibrium position; the arrows in (c) are the tip displacement vectors. The scan size is 1.5 nm by 1.5 nm in all plots.

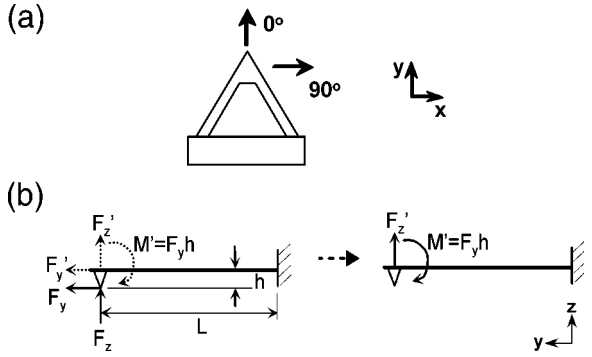

FIG. 3. (a) Top view showing the tip orientation and the scan directions. (b) Forces on the tip in the y-z plane are replaced by an equivalent force and moment on the cantilever end, neglecting the axial deformation due to F_y'.

Therefore, for a tip with either single or multiple atoms contacting with the surface, the lateral forces and the induced deflections are generally two dimensional and limited in magnitude. On the microscopic and larger scale, the nonconservative friction force in the scan direction increases proportionally with the contact area[8] whereas the conservative lateral forces remain small due to the flattening effect. Indeed the lateral force and deflection perpendicular to the scan direction are negligible compared to the relatively large scan direction friction force and surface topography variations. As a result, only the scan direction friction and the normal load are often taken into account. However, for atomic-scale imaging, the flattening effect becomes less significant and the lateral force perpendicular to the scan direction becomes comparable to the scan direction friction force. In other words, forces and deflections in all three dimensions become significant. Accordingly, the contribution from each component has to be fully represented in the AFM topographical imaging model, as will be shown in the following sections.

III. CANTILEVER AND COUPLING MECHANISM

In an optical-beam-deflection AFM, the three-dimensional atom forces are sensed by a tip attached to a microfabricated cantilever as shown in Fig. 3. The tip attachment, in the previous atomic-scale force imaging studies,[12–15] has been simply modeled as two or three uncoupled springs in the x, y, and z directions. Although these models have been successfully used to reproduce the load and stiffness dependence of the stick-slip phenomenon, etc., we believe it is too simple to capture all the important aspects of the measurement system. A coupling between the lateral force parallel to the cantilever (y direction) and the vertical deflection (z direction) needs to be taken into account. The effect of the lateral forces due to the friction and the steep surface transition in the scan direction was calculated in previous studies.[16–18] For atomic-scale imaging, since the lateral forces are two dimensional, the lateral force in the y direction could be significant regardless of the scan direction. Its effect on topographical imaging is made evident with a simple model derived below.

In this study, the deflections of the tip are measured with respect to the tip holder in which the tip is clamped. During imaging, the tip holder is stationary while the sample fixed on the scanner travels in the x, y, and z directions. The relative motion of the scanner is equivalent to the motion of the tip holder in the opposite direction. It is convenient to consider a coordinate frame fixed with respect to the scanner and discuss the relative motion of the tip and the tip holder in this coordinate frame.

Considering a cantilever always aligned with the y axis as shown in Fig. 3(a), the force on the tip can be decomposed in the x, y, and z directions—i.e., the transverse (90°), longitudinal (0°), and vertical directions. The force in the x direction is uncoupled with the forces in y and z directions (provided that the torsional deflection angle is small). In the y-z plane, the other two forces F_z and F_y can be relocated to the end of the cantilever with an additional moment $F_y h$ as shown in Fig. 3(b), where h is the tip height. The relocated lateral force F_y' can be disregarded, provided that the force is not big enough to cause buckling or significant elongation in the y direction, which is typically true for atomic-scale imaging. It is worthwhile to note here that because the lateral forces are very small (typically nN) compared to the Euler critical force of the cantilever ($\sim k_z L$, typically 10^5 nN), instability such as buckling is very unlikely to occur. Therefore the remaining force and moment are $F_z' = F_z$ and $M' = F_y h$. Under certain three-dimensional atomic forces, the small tip deflections with respect to the free load equilibrium position are given by

$$\delta = \begin{bmatrix} \delta_x \\ \delta_y \\ \delta_z \end{bmatrix} = \begin{bmatrix} 1/k_{xx} & 0 & 0 \\ 0 & h^2 L/EI & 0 \\ 0 & hL^2/2EI & L^3/3EI \end{bmatrix} \begin{bmatrix} F_x \\ F_y \\ F_z \end{bmatrix} = K^{-1} F \tag{5}$$

or $F = K\delta$, where

$$K = \begin{bmatrix} k_{xx} & k_{xy} & k_{xz} \\ k_{yx} & k_{yy} & k_{yz} \\ k_{zx} & k_{zy} & k_{zz} \end{bmatrix} = \begin{bmatrix} k_{xx} & 0 & 0 \\ 0 & EI/h^2 L & 0 \\ 0 & -3EI/2hL^2 & 3EI/L^3 \end{bmatrix}. \tag{6}$$

Here the moment of inertia I and the Young's modulus E are assumed constant along the cantilever beam length L. These assumptions are introduced for convenience of illustration. As a matter of fact, the validity of the model is insensitive to the beam geometry. Notice that in Eq. (6), k_{zy} is nonzero, accounting for the vertical displacement of cantilever beam due to the moment load $F_y h$.

When measuring the topography of the surface, the angular defection at the end of the cantilever is monitored and kept constant by a feedback loop adjusting the sample vertical position. The control law is therefore given by

$$\theta = \frac{F_z L^2}{2EI} + \frac{F_y hL}{EI}, \tag{7}$$

where θ is set to be constant and can be written as an angular deflection induced by a virtual vertical load N that is associated with the set point during the scan:

$$\frac{NL^2}{2EI}=\frac{F_zL^2}{2EI}+\frac{F_yhL}{EI},$$

$$N=F_z+F_y\frac{2h}{L}.$$

In terms of the force variation, it becomes

$$\Delta F_z=-\frac{2h}{L}\Delta F_y. \tag{8}$$

Substituting the control law, Eq. (8), into the deflection equation (5) yields a residual linear vertical deflection

$$\Delta\delta_z=\frac{L}{EI}\left(\frac{1}{3}L^2\Delta F_z+\frac{1}{2}Lh\Delta F_y\right)$$

$$=-\frac{L^2h}{6EI}\Delta F_y=-\frac{h}{2L}\frac{\Delta F_y}{k_{zz}}. \tag{9}$$

For a single-atom tip, the variation of lateral force in the longitudinal direction ΔF_y and the normal load N are on the same order of magnitude and so are the deflection term $\Delta F_y/k_{zz}$ and the vertical deflection N/k_{zz}. In contact-mode AFM imaging, a typical value of the absolute vertical deflection of the cantilever is tens of nanometers,[4,6,11] and the geometric ratio of the cantilever force sensor h/L is several hundredths. That results in a residual linear deflection of several angstroms, which is large compared to the corrugation of the surface atom topography, typically at the subangstrom level. Even for a tip with multiple atoms in contact, where the lateral forces are much reduced as shown in Sec. II, data from previous experiments[6] indicate that the conservative component of the lateral force could still cause a residual linear deflection comparable to the true topography corrugation. To see the dominant effect of ΔF_y, we replace k_{zz} by $k_{yy}=k_{zz}L^2/3h^2$ and $\Delta\delta_z$ by $z_t-(z_m+N/k_{zz})$ in Eq. (9): then, the measured height or the relative position of the tip holder is given by

$$z_m=z_t-\frac{N}{k_{zz}}+\frac{L}{6h}\delta_y. \tag{10}$$

Surprisingly, δ_y is related to z_m by a large factor of $L/6h$ (typically 5–10). In other words, deflection in the longitudinal direction appears to be amplified, showing up in the vertical direction. Meanwhile, the variation of z_t (the relative position of the tip) is close to the true topography corrugation as will be shown in Sec. IV, and N/k_{zz} is constant. Clearly, the measured topography could be dominated by δ_y even if this lateral deflection is only a fraction of the true topography corrugation ($\cong\Delta z_t$).

We further illustrate this mechanism with the load diagrams shown in Fig. 4. Under the control law, the scanner drives the net angular deflection $\Sigma\theta$ to zero while the linear deflection $\Sigma\delta$ is generally not simultaneously zero—there is a residual linear deflection which has to be compensated by the relative vertical movement of the tip holder (viewed in the coordinate frame fixed with respect to the scanner). The movement is then falsely added to the surface topography.

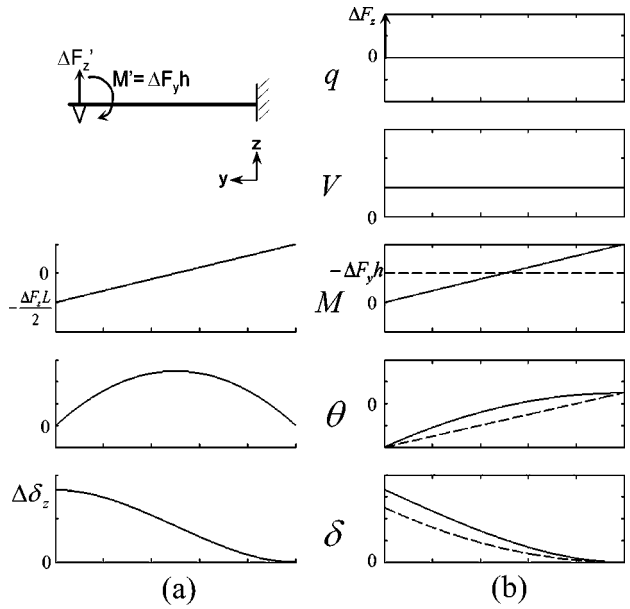

FIG. 4. Load diagrams of the cantilever under the control law, Eq. (8), are plotted in (a) and (b). The former shows the net loads and deflections. The latter shows the loads and deflections due to ΔF_z (solid line) and $-\Delta F_y h$ (dashed line). Notation: concentrate load q, shear V, moment M, angular deflection θ, and linear deflection δ.

Consequently, an error is introduced. Another minor effect of the control law is that the traced surface is no longer a constant vertical force surface but a surface satisfying $\Delta F_z=\Delta F_y(2h/L)$, which will be visualized in the next section.

An additional point is that, in reality, a small inclination angle of the cantilever β also contributes to the stiffness matrix in Eq. (6). In that case, the same analysis can be done in a rotated coordinate frame with a change of basis:

$$\hat{x}=\hat{x}',$$

$$\hat{y}=\hat{y}'\cos\beta+\hat{z}'\sin\beta,$$

$$\hat{z}=-\hat{y}'\sin\beta+\hat{z}'\cos\beta,$$

and a transformation matrix

$$S=\begin{bmatrix}1 & 0 & 0\\ 0 & \cos\beta & -\sin\beta\\ 0 & \sin\beta & \cos\beta\end{bmatrix}.$$

The stiffness matrix seen in the rotated coordinate frame is $K=SK'S^{-1}$.

IV. SIMULATION AND EXPERIMENT

This section covers the simulation model and compares the simulation results with the previous experimental data, followed by a discussion of atomic force symmetry on surface and AFM force sensor design issues.

A. Simulation model and results

The equations of the coupling mechanism from Sec. III are implemented in a simulation code. In terms of the simulation algorithm, the forces and the deflections of the tip can be calculated statically with a Polak-Ribiere-type conjugate gradient method as shown by Sasaki *et al.*[13] or dynamically solved from Newtonian equations of motion as shown by Hölscher *et al.*[12] We adopted a dynamic approach for its versatility and simplicity. As a comparison with the previous experimental data, we will show the simulation results obtained by scanning a single-atom tip over a layer of graphite substrate under a virtual constant vertical load of 0.2 nN.

A pair wise potential of Lennard-Jones form is assumed:

$$V_{\mathrm{tot}}=\sum_i 4\varepsilon\left[\left(\frac{\sigma}{r_i}\right)^{12}-\left(\frac{\sigma}{r_i}\right)^{6}\right], \tag{11}$$

where r_i is the distance from the tip atom to the atom in the graphite substrate and the parameters given are $\sigma=2.49$ Å and $\varepsilon=0.87\times10^{-2}$ eV. This model and the parameters have been used successfully to reproduce experimental results.[13] Based on the cantilever model shown in Eq. (6), the dynamics of the tip atom can be described with the following three-dimensional coupled differential equations:

$$M\begin{bmatrix}\ddot{x}_d\\ \ddot{y}_d\\ \ddot{z}_d\end{bmatrix}=\begin{bmatrix}k_{xx}&0&0\\0&k_{yy}&0\\0&k_{zy}&k_{zz}\end{bmatrix}\begin{bmatrix}x_e-x_d\\y_e-y_d\\z_e-z_d\end{bmatrix}-\begin{bmatrix}\partial V(x_d,y_d,z_d)/\partial x_d\\\partial V(x_d,y_d,z_d)/\partial y_d\\\partial V(x_d,y_d,z_d)/\partial z_d\end{bmatrix}-C\begin{bmatrix}\dot{x}_d\\\dot{y}_d\\\dot{z}_d\end{bmatrix}, \tag{12}$$

where the subscripts e and d refer to the equilibrium position (which is stationary with respect to the tip holder) and the dynamic position of the tip, respectively, in the coordinate frame that is fixed with respect to the scanner. The mass matrix and the damping matrix are in the form of a chosen constant multiplied by a unit diagonal matrix, respectively, $M=mI$ and $C=cI$. The components of both matrices are assumed independent and equal in the three dimensions whereas the other two terms, the partial derivative of the potential and the stiffness matrix K, as described in Sec. III, introduce coupling. The simulation is conducted when the tip scans are in the 90° direction (x axis). The forces are calculated using Eq. (12) and the tip holder height is constantly adjusted so that the control law in Eq. (8) is satisfied. As predicted by Eq. (10), we obtain a ''topography'' map as shown in Fig. 5(a), dominated by the amplified 0° direction deflection (longitudinal direction) as shown in Fig. 5(d).

These simulated images agree well with the previous experimental results[6,11] in terms of the triangular shape of the ''atom images'' and the well-known puzzling feature of the ''resolution of every other atom.'' In particular, the images in Figs. 5(a) and 5(c) precisely reproduce the simultaneously measured ''topography'' and the friction force map presented by Run and Buhshan.[6] However, the peaks appearing in the ''topography'' map are interpreted here as *neither images of "every other atom" nor that of any atom but as the maxima of the longitudinal direction lateral force*. Since the longitudinal direction lateral force has only one peak per hexagonal carbon ring, the ''topography'' images display a trigonal structure, which were previously interpreted as images of the type-B carbon atoms in numerous studies. The phase shift between the ''topography'' peaks and the friction peaks in the scan direction is thus interpreted as the phase shift between the peaks of the lateral force in the longitudinal direction and that in the transverse direction (also the scan direction in this case). Both types of peaks are found between the center and the edge of the hexagonal ring, where the lateral component of the potential gradient is maximal. With this concluded, it is straightforward, as shown in Fig. 6, to determine where the graphite atoms actually are in the ''topography'' image or in the friction force image. Another interesting agreement is that the corrugation amplitude of the ''topography'' measured by Run and Bhushan was 0.2 nm which is much larger than the value from theoretical calculation[19] and experiments of He scattering,[20] ~0.3 Å. The above simulation reproduces both values, corresponding, respectively, to the variation of z_m and the variation of z_t

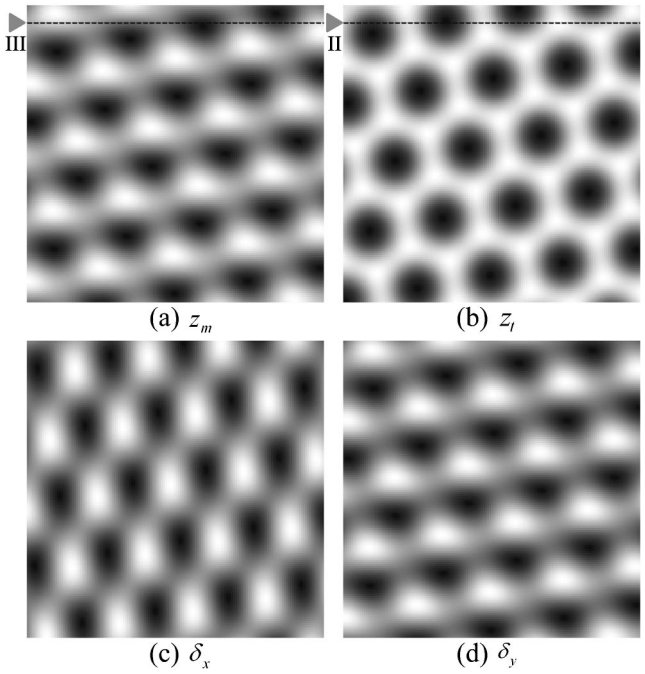

FIG. 5. Simulation results: (a) the measured ''topography'' z_m, (b) the actual tip traced surface z_t, (c) the deflection in the x direction, δ_x, and (d) the deflection in the y direction, δ_y. Clearly, z_t is quite different from z_m which is in fact dominated by δ_y due to the coupling and application mechanism, as explained in Sec. III. In (c), deflection in the x direction is a true measure of the lateral force in the same direction because it is uncoupled. Simulation was performed with a virtual constant load of 0.2 nN; cantilever linear deflection ~17 nm, and tip-cantilever dimensions are $L=100$ μm and $h=3$ μm. When the scan speed is small enough and the transient effect dies out, the dynamic simulation gives identical results regardless of the choice of the mass and damping value. However, various masses and damping coefficient (for example, single-atom mass and arbitrary light damping) have been tested merely to reduce the simulation time.

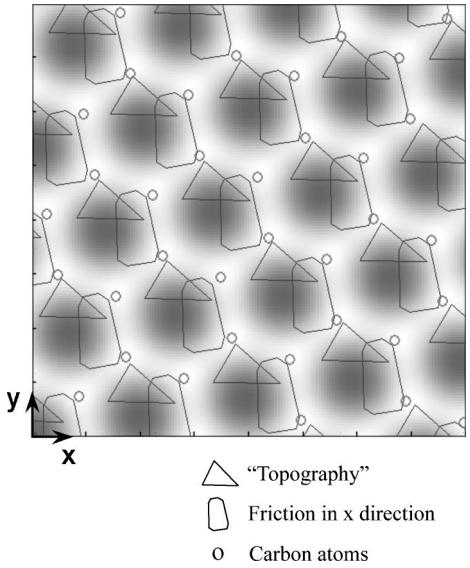

FIG. 6. Schematic showing maxima in the simultaneously measured ''topography'' (longitudinal direction lateral force map) and friction with a background of the true topography and the carbon atoms (note that the A site and the B site are not distinguished in the calculation).

(approximately). The anomalously large corrugation is attributed to the coupling and amplification mechanism described by Eq. (10).

The results presented above explain the so-called ''resolution of every other atom'' issue in various aspects. In the previous studies, several other possible explanations had been proposed: briefly, (1) the asymmetric atomic structure, (2) tips with multiple contact atoms,[21,22] (3) a possible graphite flake attached to the end of the tip,[8] and (4) the tip sticks at the hollow sites and skips the carbon atom sites due to the stick-slip movement.[12] [For a detailed review of (1)–(3) see Ref. 6.] A difficulty these theories have in common is to explain why the ''resolution of every other atom'' occurs in some experiments whereas the entire hexagonal carbon ring was observed in others. Indeed, those successful observations[2,3] of the hexagonal ring tend to exclude the explanation based on the asymmetric atomic structure because if a significant force difference does exist inherently between the A sites and the B sites for some experiments, it should exist for all experiments. As a matter of fact, the theoretical caculations[23–25] showed such a force difference is very small and both types of atoms should be visible to the AFM tip. Multiple-atom tips and attached graphite flakes are possible: however, the corner of the cantilever used by Binnig *et al.*[2] should not be superior to a sharp tip in terms of avoiding these possibilities, yet the hexagonal carbon ring was seen with the former but not the latter.

Although the tip could stick at the hollow sites for most of the time during scanning, the sticking regions should be low in height. On the other hand, the edge of the hexagonal carbon ring should lift the tip to higher positions although with a reduced ''position probability density.'' Therefore, the consequence of the stick-slip movement for topographical imaging should be bright but thin hexagonal rings instead of the

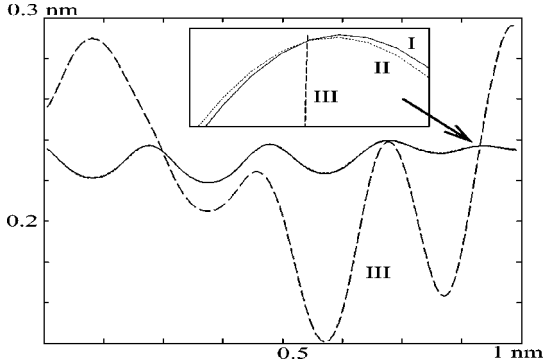

FIG. 7. Comparison of the traced lines from the three surfaces (all surfaces are viewed in the coordinate frame fixed with respect to the scanner): (I) constant vertical force surface from Fig. 8(a), (II) constant angular deflection surface from Fig. 5(b), and (III) tip-holder-traced surface from Fig. 5(a).

''resolution of every other atom.'' Interestingly, this conjecture agrees very well with the experimental results of Marti, Drake, and Hansma[3] where such bright but thin hexagonal rings were observed with a unique force sensor design. In their experiment, a sharp diamond tip with a height of 0.5 mm was used; stick-slip very likely occurred. However, the tip was glued to sensing wires with both ends clamped instead of a cantilever—which was a setup free of the residual deflection: therefore, the relatively weak signal of the hexagonal rings could be observed without being screened by the dominating lateral force signal as shown in Fig. 5. The same was true for the setup used by Binnig *et al.*,[2] a tipless cantilever monitored by an STM, except that the hexagonal carbon rings they observed were thicker, probably due to the higher lateral stiffness of the tipless cantilever. Not only are these two cases consistent with an explanation based on the residual linear deflection, but also they provided experimental proof that imaging the entire hexagonal structure is possible in the absence of the residual linear deflection induced by the two-dimensional lateral forces. In previous studies,[6,12] the possible role of the two-dimensional lateral forces in topographical or lateral force imaging had been brought to attention, but the discussions were focused on their influence on the movement of the tip—i.e., the tip-traced surface. It is shown graphically in the following that a more significant influence is on another traced surface, the tip-holder-traced surface.

B. Three traced surfaces

The term ''topography'' has been referred to as the constant vertical force surface which, unfortunately, is not the one being detected in most cases. Instead, two other surfaces—namely, the constant angular deflection surface (the tip-traced surface) and the measured ''topography'' (the tip-holder-traced surface or inversed-scanner-traced surface)—are actually being traced, and the latter is the only one recorded by the instrument. With simulations, one could put all three surfaces into perspective at the same time. From each of the above three surfaces, a trace line is taken at the same location and compared as shown in Fig. 7. Interest-

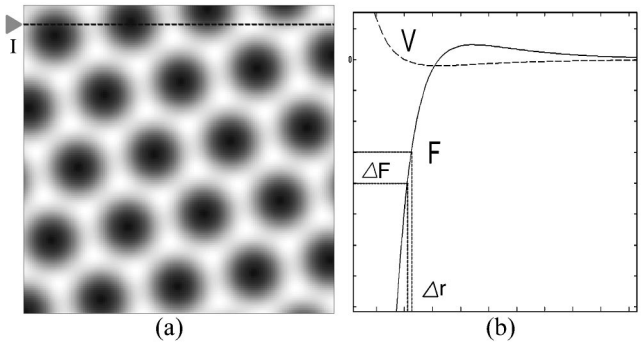

FIG. 8. (a) Calculated real constant vertical force surface (true topography) for $F_z=-0.2$ nN. (b) Schematic showing that fast-growing short-range repulsive force results in an increasingly large force gradient.

ingly, the difference between the constant vertical force surface and the constant angular deflection surface is negligible despite the fact that $\Delta F_z=\Delta F_y(2h/L)$ could be considerably large. A blessing is that, in the short-range repulsive force regime, by increasing the normal load, the amount of deflection it takes to accommodate a certain force variation is decreased as shown in Fig. 8. Therefore surfaces I and II are very close. Nevertheless, an enlarged view in Fig. 7 shows how the longitudinal direction lateral force slightly alters the trace line of the tip depending on the sign of this force. However, the amplitude of the corrugation remains unaffected because the longitudinal direction force vanishes at the points where the vertical force reaches its maxima and minima. These points of extremum are also on surface III because the residual linear deflection which causes surface III to deviate vanishes when the longitudinal direction force vanishes. Other than these points, surface III, the measured ''topography'' and surface II, the tip-traced surface, generally deviate from surface I, and the former could have a much larger deviation, as shown in Fig. 7 and Eq. (10).

Besides these three traced surfaces, there could be other traced surfaces, depending on the design of the AFM. An example is given in Sec. IV D for AFM's with linear deflection directly sensed by STM's. In principle, the tip traced surface is determined by the control law while the tip-holder-traced surface is the sum of the tip-traced surface and the cantilever residual deflection.

C. Symmetry of atom force pattern on surface

A challenging question is that if the measured ''topography'' surface is dominated by the residual cantilever deflection in optical-beam-deflection AFM's as shown above, why is it that ''topography'' images correctly representing the surface lattice structure have been reported such as for NaCl?[4] That could be explained in two ways. First, we noticed that in some measurements, tipless cantilevers were used;[2,4] therefore, the moment load due to the tip height vanishes. However, that alone does not guarantee a zero residual deflection because the inevitable slight inclination of the cantilever also introduces coupling. Another interesting relevant observation is that taking a friction force measurement of the

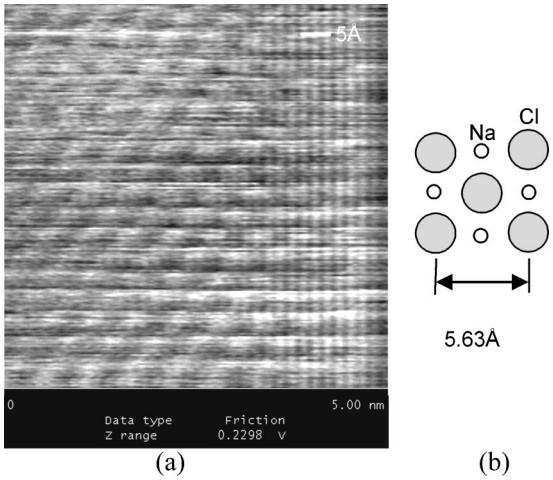

FIG. 9. Friction force map (band pass filtered) of NaCl (001) surface shows the same lattice structure as would be shown by true constant vertical force map. Image was obtained with Digital Instrument MultiMode AFM (Ref. 28) when scanning in the 90° direction.

surface of certain materials, the lateral force map pattern could be the same as that of the true topography. An example is the NaCl (001) surface as shown in Fig. 9. The friction force map displays the same fcc lattice structure as would be seen if the true topography (or vertical force map) is correctly measured or simulated. Therefore, fcc structure could be observed for a NaCl (001) surface even if the image is dominated by lateral forces. For such surfaces, the atoms' force pattern appears to have a higher degree of symmetry (three dimensional). Clearly, the same kind of symmetry does not hold for the graphite basal plane surface—the lateral force distributions show only three maxima per hexagonal ring[6,26,27] while the topography (or the vertical force map) shows six.[2,3] However, it has to be pointed out that for those surfaces with three-dimensional symmetric atom force patterns, not all force images directly tell us the real atom locations because of the phase shift between the vertical force maxima and the lateral force maxima and between the maxima of the two lateral forces as well. Therefore, the dominant force has to be identified before the real atom locations can be determined.

D. Further discussions

Microfabricated cantilevers are sensitive force sensors with two degrees of deflection freedom which are bending and torsion, but the surface forces on the atomic scale are significant in all three dimensions. The torsion direction is well decoupled from the other two but bending is always affected by one or both lateral forces regardless of the cantilever orientation and scan direction. In order to measure the vertical force, the challenge is to decouple it from the longitudinal direction force. Unfortunately, this is not being accomplished by the constant optical-beam-deflection scheme because of the nonzero residual linear deflection $\Delta\delta_z$ as given in Eq. (9). As a matter of fact, if we trace back to the early days of the AFM, the first design of the AFM should be

free of this drawback because it directly drives $\Delta\delta_z$ to zero with a STM. In that case the control law is equivalent to $\Delta F_z = \Delta F_y 3h/2L$. Although it does not represent the same surface as $\Delta F_z = 0$ does, the difference can be well neglected, similar to the case shown in Fig. 8. However, in that design, since the STM is used to monitor the elastic deformation of a cantilever, the imaging might be affected by the limitations of the STM. For example, in most STM images, only one maximum is observed per unit graphite unit cell.[29–32] Similar images were observed for some of AFM's using STM's to monitor the deflection.[33] Different from the cantilever approach, a unique design[3] in the early days of the AFM had successfully decoupled the vertical and longitudinal directions by fixing both ends of the tip support wires. With that design, although the setup is ''relatively crude'' as the author commented, they were able to observe the hexagonal ring of a graphite unit cell. This result together with the graphite image obtained by Binning *et al.*[2] with a tipless cantilever monitored by a STM provides an experimental basis on which we could be optimistic about obtaining true atom images once the coupling mechanism issue is resolved.

To resolve this issue, eliminating the residual linear deflection is the key. It would be an elegant solution if the moment of inertia of the cantilever beam can be carefully designed so that the vertical deflections induced by the vertical force and the moment can be canceled out at the same time when the angular deflection is driven to zero. However, it can be proved graphically that this demands a negative moment of inertia, which is not practical. Nevertheless, the residual linear deflection can be reduced by designing the moment of inertia to vary along the cantilever length. Other resolutions could be direct control of the vertical linear deflection or fixing the other end of the cantilever as was done in the early AFM designs. In that case, detection of the vertical deflection and maintaining the sensitivity of the sensor need to be carefully considered. Last but not least, an alternative resolution is to do nothing, since the lateral force variation is much easier to detect than the normal force variation, so why not just be aware of the fact and reconstruct the actual atom locations from the lateral force maps as shown in Fig. 6? Furthermore, if the lateral force is being detected, a LFM could be designed for high sensitivities to the lateral forces, just as a cantilever parallel to the surface is designed to be most sensitive to the normal force.

V. CONCLUSIONS

In this paper we emphasize the three-dimensional nature of the atomic forces and the induced AFM tip deflections. A simple model is introduced to describe a coupling and amplification mechanism in an optical-beam-deflection AFM due to the two-dimensional lateral forces that become significant on the atomic scale. It is shown that although the difference between the true topography (the constant vertical force surface) and the tip-traced surface (the constant angular deflection surface) is generally subtle, the difference between these surfaces and the measured ''topography'' (the tip-holder-traced surface or inversed-scanner-traced surface) can be significant due to a residual linear deflection. As a result, we could interpret previously obtained ''topography'' images with the so called ''resolution of every other atom'' as maps of the lateral force in the longitudinal direction; the true locations of the atoms with respect to the apparent peaks can be determined. This interpretation can explain not only why the ''resolution of every other atom'' was observed in some experiments but also why the entire hexagonal ring was observed in others. We further clarify with experiment that certain surfaces have similar force patterns in all three dimensions such as NaCl (001) while others have less symmetry in the atom forces such as the basal plane of graphite. For the former, caution has to be taken in interpreting which force is responsible for the apparent peaks and in turn where the atoms actually are with respect to the apparent peaks. Finally, a few possible directions of resolving the residual linear deflection issue are discussed.

ACKNOWLEDGMENTS

Support for W.L.W. and S.J.H. was sponsored in part by the U.S. Army Dual Use Science and Technology Program (DUST) Award No. DAAE07-01-3-0002. R.C. was supported in part by U.S. Department of Energy Grant No. FG02-03ER46023.

[1] G. Binnig, C. F. Quate, and Ch. Gerber, Phys. Rev. Lett. **56**, 930 (1986).
[2] G. Binnig, Ch. Gerber, E. Stoll, T. R. Albrecht, and C. F. Quate, Europhys. Lett. **3**, 1281 (1987).
[3] O. Marti, B. Drake, and P. K. Hansma, Appl. Phys. Lett. **51**, 484 (1987).
[4] G. Meyer and N. M. Amer, Appl. Phys. Lett. **56**, 2100 (1990).
[5] G. Meyer and N. M. Amer, Appl. Phys. Lett. **57**, 2089 (1990).
[6] J. Ruan and B. Bhushan, J. Appl. Phys. **76**, 5022 (1994).
[7] G. Binnig, Ultramicroscopy **42–44**, 7 (1992).
[8] C. M. Mate, G. M. McClelland, R. Erlandsson, and S. Chiang, Phys. Rev. Lett. **59**, 1942 (1987).
[9] S. Fujisawa, Y. Sugawara, S. Ito, S. Mishima, T. Okada, and S. Morita, Nanotechnology **4**, 138 (1993).
[10] S. Fujisawa, E. Kishi, Y. Sugawara, and S. Morita, Phys. Rev. B **51**, 7849 (1995).
[11] S. Fujisawa, K. Yokoyama, Y. Sugawara, and S. Morita, Phys. Rev. B **58**, 4909 (1998).
[12] H. Hölscher, U. D. Schwarz, O. Zwörner, and R. Wiesendanger, Phys. Rev. B **57**, 2477 (1998).
[13] N. Sasaki, K. Kobayashi, and M. Tsukada, Phys. Rev. B **54**, 2138 (1996).
[14] J. Shimizu, H. Eda, M. Yoritsune, and E. Ohmura, Nanotechnology **9**, 118 (1998).
[15] H. Hölscher, U. D. Schwarz, and R. Wiesendanger, Surf. Sci. **375**, 395 (1997).
[16] A. J. den Boef, Rev. Sci. Instrum. **62**, 88 (1990).
[17] M. Radmacher, R. W. Tillmann, M. Fritz, and H. E. Gaub, Sci-

ence **257**, 1900 (1992).
[18] R. J. Warmack, X.-Y. Zheng, T. Thundat, and D. P. Allison, Rev. Sci. Instrum. **65**, 394 (1994).
[19] A. Selloni, P. Carnevali, E. Tosatti, and C. D. Chen, Phys. Rev. B **31**, 2602 (1985).
[20] W. E. Carlos and M. W. Cole, Surf. Sci. **91**, 339 (1980).
[21] H. A. Mizes, S. I. Park, and W. A. Harrison, Phys. Rev. B **36**, 4491 (1987).
[22] S. A. C. Gould, K. Burke, and P. K. Hansma, Phys. Rev. B **40**, 5363 (1989).
[23] F. F. Abraham and I. P. Batra, Surf. Sci. **209**, L125 (1989).
[24] I. P. Batra and S. Ciraci, J. Vac. Sci. Technol. A **6**, 313 (1988).
[25] L. Xu, X. W. Yao, L. P. Zhang, M. Q. Li, and F. J. Yang, Phys. Rev. B **51**, 10 013 (1995).
[26] M. Tosa, Adv. Colloid Interface Sci. **71–72**, 233 (1997).
[27] W. Allers, A. Schwarz, U. D. Schwarz, and R. Wiesendanger, Appl. Surf. Sci. **140**, 247 (1999).
[28] MutiMode SPM, Digital Instruments, Santa Barbara, CA.
[29] S. Park and C. F. Quate, Appl. Phys. Lett. **48**, 112 (1986).
[30] G. Binnig, H. Fuchs, Ch. Gerber, H. Rohrer, E. Stoll, and E. Tosatti, Europhys. Lett. **1**, 31 (1986).
[31] H. J. Mamin, E. Ganz, D. W. Abraham, R. E. Thomson, and J. Clarke, Phys. Rev. B **34**, 9015 (1986).
[32] D. Tomanek, S. G. Louie, H. J. Mamin, D. W. Abraham, R. E. Thomson, E. Ganz, and J. Clarke, Phys. Rev. B **35**, 7790 (1987).
[33] T. R. Albrecht and C. F. Quate, J. Appl. Phys. **62**, 2599 (1987).